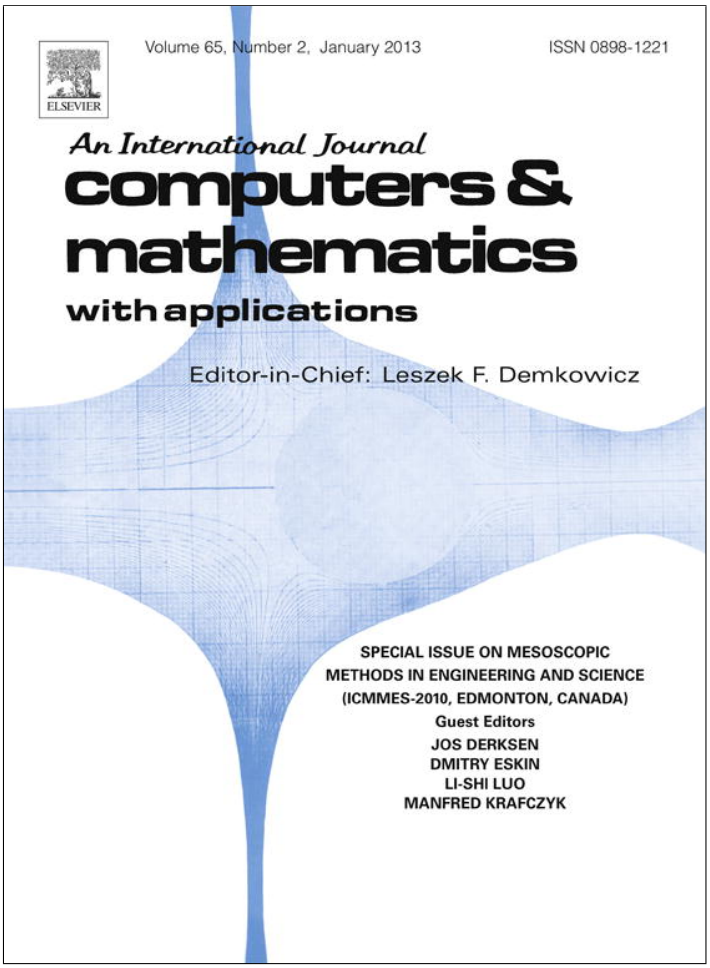

Computers and Mathematics with Applications 65 (2013) 287–295

Contents lists available at SciVerse ScienceDirect

Computers and Mathematics with Applications

journal homepage: www.elsevier.com/locate/camwa

Simulation of a mannequin's thermal plume in a small room

Xinli Jia [a], John B. McLaughlin [a,*], Jos Derksen [a,b], Goodarz Ahmadi [a]

[a] Clarkson University, Potsdam, NY 13699, USA

[b] University of Alberta, Edmonton, Alberta TG6 2V4, Canada

ARTICLE INFO

Keywords:
Thermal plume
Heated mannequin
Small room
Particle trajectories
Lattice Boltzmann method

ABSTRACT

Simulation results are presented for the buoyancy-driven flow in a small room containing a seated mannequin that is maintained at a constant temperature. The study was motivated, in part, by a published experimental study of the thermal plume around a human subject. The results presented are a step toward the goal of using DNS to develop a more detailed understanding of the nature of the flow in the thermal plume created by humans modeled here as heated mannequins. The results were obtained without using sub-grid scale modeling and are helpful in establishing the resolution requirements for accurate simulations. It is seen that the results for the highest resolution grid are in reasonable quantitative agreement with a published experimental study of a human subject's thermal plume. The results for the velocity field are used to compute the trajectories of small particles in the room. Results are presented for the trajectories of five-micrometer solid particles that are initially dispersed near the floor in front of the mannequin. The simulation results show that the buoyancy-driven flow around the mannequin is effective at dispersing the particles over a large portion of the room.

1. Introduction

This paper presents simulation results for the velocity and temperature fields in a small room containing a heated mannequin. The study was motivated in part by the work of Craven and Settles [1]. Cravens and Settles performed an experimental study of the thermal plume around a standing human subject. The ceiling of the room in which the person was standing was 3.25 m above the floor, and the subject was 1.73 m tall. The subject stood in a rectangular box that measured $1.00 \times 0.81 \times 0.51$ m. The temperature on the surface of the subject's clothing was measured at 40 locations, and the average value was found to be 26.6 °C; the average skin temperature based on the same 40 locations was 31.8 °C. The air in the room was thermally stratified, and varied from 20 °C at the floor to 22.5 °C at the ceiling. Theater fog, consisting of 5 μm particles, was used to visualize the flow around and above the subject. PIV measurements using turbulent eddies as "particles" were used to measure the air velocity at various locations. Cravens and Settles obtained results for the magnitudes of the time-averaged velocities at various points around the mannequin; they did not report values of the turbulent intensities. The largest velocity was 0.24 m/s, and it occurred at a distance equal to 0.43 m above the subject's head (2.16 m above the floor).

Cravens and Settles also reported the results of Reynolds-averaged Navier–Stokes (RANS) simulations of the flow around a simplified model of the human subject in their experiments. Thermal stratification could be incorporated into their simulations. For the stratification in their experiment, the average air temperature was 21.3 °C, and the mannequin's surface temperature was 26.6 °C. On the basis of previous experimental studies of the transition to turbulence on vertical heated surfaces (see, for example, Incropera and DeWitt [2]), they assumed that the transition occurred when the Rayleigh number

* Corresponding author. Tel.: +1 315 268 6663.
E-mail address: jmclau@clarkson.edu (J.B. McLaughlin).

0898-1221/$ – see front matter © 2011 Elsevier Ltd. All rights reserved.
doi:10.1016/j.camwa.2011.06.056

was 10^9, which corresponds to a height equal to 1.2 m above the floor. Their simulations predicted that the largest vertical velocity was 0.2 m/s, and it occurred at 2.12 m above the floor. Without stratification, the largest vertical velocity was found to be 0.3 m/s and it occurred at approximately 2.8 m above the floor.

The simulations to be reported were performed for a seated mannequin in a room that is much smaller than the room in which the above experiments were performed. Since one goal of the study was to evaluate the feasibility of using DNS to study the human thermal plume, the smaller size of the room is important. As in the work reported by Craven and Settles, no air enters or leaves the room. The choice of the room was motivated by experiments carried out with one or more medical mannequins in a small room that were reported by Marr [3,4] and Spitzer et al. [5]. In these studies, the mannequin(s) could be heated or unheated and breathing was also included in some experiments. A significant difference between these experiments and the results to be reported is that, in all of the experiments, air flowed into the room through a floor vent and exited through a ceiling vent. To include the forced convection in a simulation, a finer grid would be needed to account for the small scale fluctuations in the flow entering the room. Alternatively, one could follow the approach used by Abdilghanie et al. [6] who used large eddy simulation (LES) to compute the flow in the above room. Earlier LES studies of indoor airflows were reported by Davidson and Nielsen [7], Zhang and Chen [8,9], and Jiang and Chen [10]. In addition to conducting measurements of velocity and temperature, 5 μm particles were released near the floor and the effectiveness of a mannequin's thermal plume in dispersing the particles was investigated. In the present paper, results are also presented for the motion of 5 μm particles that are released in a volume near the floor and directly in front of the mannequin. The simulation results show that the thermal plume is effective in lifting the near floor particles and bringing them to the breathing zone as well as dispersing the particles over a large volume of the room.

The present study addresses a set of issues different than those considered in the study by Abdilghanie et al. [6]. The focus of the present study is on the flow driven by the thermal plume created by a single mannequin that is seated in the room. No air either enters or leaves the room. This reduces the computational requirements for an accurate simulation since it eliminates the need to simulate the small eddies that enter the room through the inlet flows. Despite this simplification, the thermal plume of a mannequin or person still presents significant computational challenges for accurate simulations. Features such as the largest instantaneous vertical velocities directly above the mannequin's head were sensitive to the spatial resolution used in the study.

Although the simulations to be discussed were performed for the same room as was considered by Marr et al. and Spitzer et al., there are several significant differences. First, a simple block model of a seated mannequin was used in the simulation instead of the anatomically realistic mannequin used in the above study. Second, furniture was not included in the simulation. Finally, the temperature of the mannequin was chosen to be 5 °C warmer than the initial air temperature (i.e., the mannequin's surface temperature was 25 °C instead of 31 °C and the initial air temperature was chosen to be 20 °C). This choice was motivated by the experiments reported by Craven and Settles [1].

2. Formulation of the problem

2.1. Geometry and boundary conditions

The room for which the simulations were performed is shown in Fig. 1, which also shows the Cartesian coordinate system that will be used in what follows. The dimensions of the room's interior are 2.4 m × 1.8 m × 2.45 m in the x, y, and z directions, respectively. A layer of insulating material of thickness 0.11 m was added above the ceiling so that the temperature of the ceiling could vary with time as the air above the mannequin became warmer. The room was equipped with a single inlet located on the floor in front of the mannequin and a single outlet located on the ceiling behind the mannequin. As a consequence of the insulation above the ceiling, a short rectangular duct preceded the outlet. In the present study, however, no air either entered or left the room. Fig. 1 also shows the simple block model of a mannequin that was used in the simulation. The mannequin is centered on the geometrical symmetry plane ($x = 0.9$ m) of the room. The widths of the mannequin's torso in the x and y directions were 0.44 m and 0.72 m, respectively, and the top of the mannequin's head was 1.24 m above the floor. The distance between the mannequin's head and the ceiling was 1.21 m, which was somewhat smaller than the distance between the top of the human subject's head and the ceiling in the experiments of Craven and Settles (1.52 m).

At the initial time, the temperatures of the air, floor, walls, and ceiling were set to 20 °C. The mannequin's temperature was 25 °C, and this temperature was imposed throughout the simulation. Isothermal boundary conditions were imposed on the floor and walls. Although one would expect some warming of these surfaces over time, the simulations to be discussed were performed for sufficiently short periods of time that it is unlikely that these boundary conditions would greatly affect the results to be reported. The temperature of the ceiling was not imposed after the initial instant in time so that its temperature could gradually rise due to the thermal plume above the mannequin. Thermal conduction was permitted through a layer of thermal insulation above the ceiling that was 0.11 m thick. The air was initially motionless throughout the room. Any motion of the air was, therefore, caused by thermal buoyancy.

2.2. Numerical methods

The simulations were performed with a lattice Boltzmann method (LBM) that was developed by Inamuro et al. [11,12]. The Boussinesq approximation was used to incorporate buoyancy into the Navier–Stokes equation. There are two classes

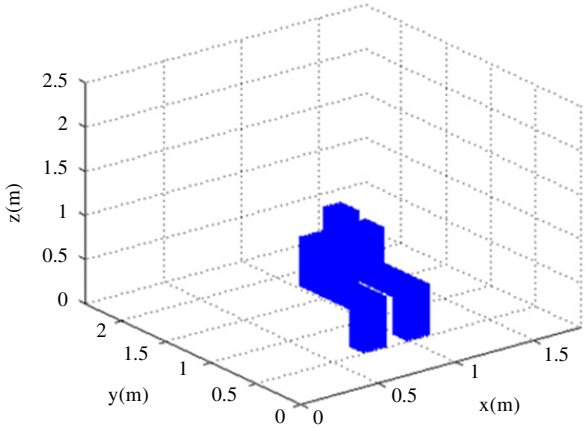

Fig. 1. Geometry of the room and the mannequin.

Table 1
The three grids used in the simulations.

Grid	N_x	N_y	N_z	Δx (m)	Δt (s)	Simulation time (s)	Max. $v_{z,m}(t)$ (m/s)	Time (s)
1	90	120	128	0.02	0.005	600	0.254	50
2	180	240	256	0.01	0.0025	150	0.327	117.5
3	270	360	384	0.00667	0.001667	683	0.379	167

of "thermal" LBMs: (1) multi-speed methods [13–15] and (2) passive scalar methods [13,14]. The approach described by Inamuro et al. [12] falls into the passive scalar approach group. An advantage of the passive scalar approach is that it is possible to freely specify the Prandtl number of the fluid and it is more stable than multi-speed methods. Inamuro et al. [12] also showed that their method produced excellent agreement with the theoretical value of the critical Rayleigh number for the onset of Rayleigh–Benard thermal convection. The methods of Inamuro et al. were chosen for the simulations to be discussed because of their relative simplicity (comparable to that of the BGK LBM) and the fact that the authors had prior experience with them. It is possible that the other methods summarized above as well as recent developments, such as the "double-population" thermal LBMs discussed by Nor Azwadi and Tanahashi [16], might have advantages relative to the method chosen in the present work. A more detailed discussion of thermal LBMs may be found in the recent paper by Liu et al. [17].

One advantage of the Inamuro et al. LBM is that it is possible to specify the Prandtl number; in some versions of the LBM, the Prandtl number is constrained to be unity. The Prandtl number of air was taken to be 0.71 in the simulations to be reported.

The simulations were performed on three uniform cubic grids. The numbers of grid points in each of the three orthogonal directions, the values of the grid space, $\Delta x = \Delta y = \Delta z$, and the time step, Δt, are summarized in Table 1. Simulations were performed for sufficient time that the velocity field over the mannequin's head reached an approximate statistical steady state. The total integration times are given in Table 1.

The artificial force method described by Derksen and Van den Akker [18] was used to enforce rigid no-slip boundary conditions at all points on the surface of the mannequin and on the ceiling and interior of the exit duct. The values of the velocity at points on the surface of the mannequin and its interior were checked periodically to ensure that they were sufficiently small.

The simulations were performed on the Intel 64 cluster ("Abe") at the National Center for Supercomputer Applications (NCSA). The code was parallelized, and the simulations were performed on 8, 16, and 32 processors, respectively for grids 1, 2, and 3. The clock time for a simulation was approximately inversely proportional to the number of processors; when 32 processors were used instead of 16 processors for a simulation on grid 3, the clock time was reduced by nearly a factor of 2.

Simulations were performed for the grids in Table 1 to determine the effect of spatial resolution on the computed results. For each simulation, the velocity and temperature fields were stored every 1.67 s (1000 time steps). Then, the largest value of the vertical velocity, $v_{z,m}(t)$, was determined for each of the stored velocity fields. Typically, the largest value of the vertical velocity occurred at a point directly above the mannequin's head. This point was located in or near the geometrical symmetry plane of the room ($x = 0.9$ m). The z coordinate of the relevant point at which the instantaneous maximum occurred varied significantly with time—by as much as a meter, but was consistently located above the mannequin's head throughout the simulation. The maximum values of $v_{z,m}(t)$ and the times at which they occurred are recorded in the last two columns of Table 1.

The simulations for all three grids appear to reach an approximate steady state after about 60 s. When $v_{z,m}(t)$ is averaged over the time interval from 60 to 150 s, the averaged values are 0.198, 0.321, and 0.358 m/s for grids 1, 2, and 3, respectively.

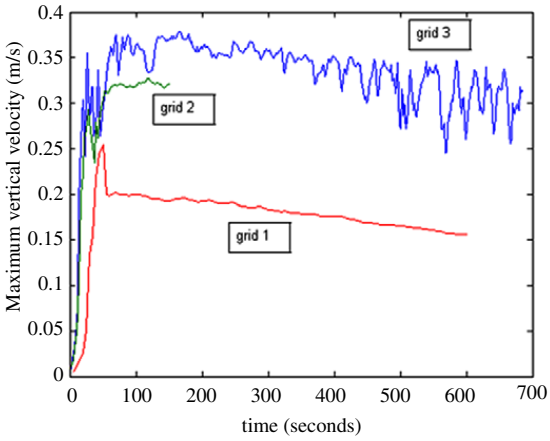

Fig. 2. The maximum vertical velocity is plotted versus time for grids given in Table 1.

On the basis of these values, it is clear that the spatial resolution for grid 1 is inadequate. Since the difference between the values for grids 2 and 3 is still significant, it is not clear that grid 3 has sufficient resolution to be considered a DNS. A simulation with a larger number of grid points will be needed to determine whether or not this is the case.

3. Results

3.1. Velocity and temperature fields

Results are shown both for instantaneous and time-averaged fields and for root mean square fluctuations. For grid 3 the averages were performed over the time interval 568 to 683 s. During this period of time, the air in the upper portion of the room had warmed sufficiently that, as may be seen in Fig. 2, the largest local vertical velocities had decreased noticeably from their maximum value. The results obtained with grids 1 and 2 are also shown for comparison. It may be seen that $v_{z,m}(t)$ quickly reaches a local maximum within roughly 30 s. It then gradually increases to 0.379 m/s. It eventually reaches an approximate statistical steady state after roughly 100 s. At still larger times, however, it may be seen that the maximum velocity gradually decreases due to the warming of the air in the upper portion of the room, which reduces the buoyancy force. In what follows, results are shown only for grid 3.

The points at which the instantaneous largest values of the vertical component of velocity occur vary widely. In their experiments with a human subject, Cravens and Settles identified the point at which the time-averaged vertical component of velocity, $\langle v_z \rangle$, had its maximum value. The point was located at approximately 0.43 m above the subject's head, and the time-averaged vertical component of the velocity at that location was 0.24 m/s.

To compare the results obtained from the present simulation with the above results, the vertical velocity was time-averaged over the time interval 567 to 683 s. It was found that the maximum value of $\langle v_z \rangle$ occurred at a point that was 0.53 m above the mannequin's head and that the value of the maximum was 0.226 m/s. Given the differences in geometry between the experiment and the present simulation, the agreement is reasonably good. Fig. 3 shows contour plots of the time-averaged vertical component of velocity and the corresponding RMS fluctuations in the plane $y = 1.12$ m, which passes through the center of the mannequin's upper body. The slight asymmetry seen in the plots is due to the limited amount of time-averaging, which was dictated by the fact that the thermal stratification of the air in the room is slowly changing in time. Fig. 4 shows the time-averaged vertical component of velocity and the corresponding RMS fluctuations in the geometrical symmetry plane of the room, $x = 0.9$ m. Figs. 3 and 4 show that the largest vertical velocities and the regions of strongest turbulent fluctuations roughly coincide and are located directly above the mannequin's head. The RMS fluctuations are very small in the lower half of the room.

In Fig. 5, $v_z(t)$ is plotted over the time range 567 to 683 s at three points in the symmetry plane of the mannequin shown in Fig. 3. The points are located along the symmetry line at $z = 1.50$, 1.77, and 2.11 m. The corresponding distances above the mannequin's head are 0.26, 0.53 and 0.87 m. The second of the above points is the location at which the time-averaged vertical component of velocity has its maximum value. For reference, the ceiling is located at $z = 2.45$ m (1.21 m above the mannequin's head.)

Fig. 6 shows the instantaneous velocity field at $t = 143.4$ s in the geometrical symmetry plane of the room ($x = 0.9$ m) and the plane $y = 1.12$ m, which passes through the torso and head of the mannequin. Only 1/9 of the vectors are shown for clarity. It may be seen that the flow is relatively complex in the region above the mannequin and much smoother in the lower part of the room, which is consistent with the behavior of the RMS fluctuations shown in Figs. 3 and 4.

Fig. 7 shows the time-average temperature field and the RMS temperature fluctuations in the plane $x = 0.9$ m. It may be seen that the largest temperatures and RMS temperature fluctuations occur in roughly the same region as the largest vertical velocities and RMS vertical velocity fluctuations. Fig. 8 shows the same quantities in the plane $y = 1.12$ m.

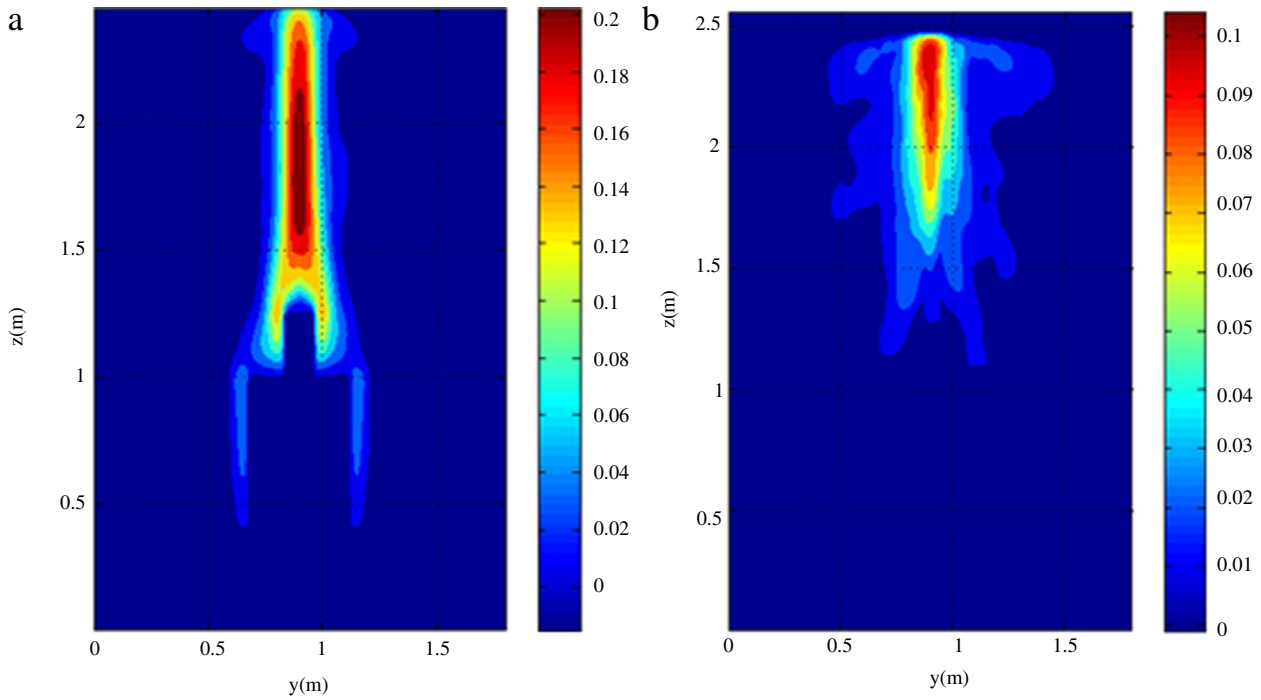

Fig. 3. The time-averaged vertical component of velocity (a) and the RMS fluctuations in the vertical component of velocity (b) are shown in the plane $y = 1.12$ m.

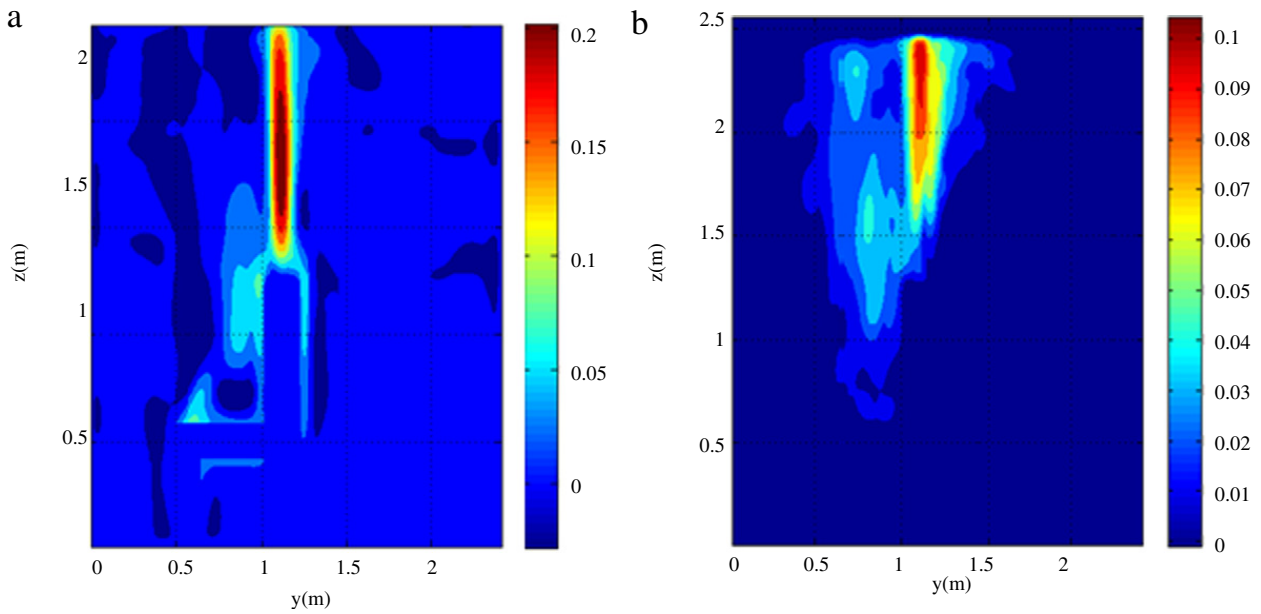

Fig. 4. The time-averaged vertical component of velocity (a) and the RMS fluctuations in the vertical component of velocity (b) are shown in the plane $x = 0.9$ m.

As noted earlier, the temperature field in the room does not achieve a true steady state during the time of the simulation because of the gradual warming of the air in the upper portion of the room, which reduces the buoyancy force. Fig. 9 shows the horizontally averaged final temperature fields at 300, 501, and 683 s. In all three cases, the horizontally averaged temperature reaches a maximum at the ceiling. The ceiling temperature slowly increased with time. This behavior is due to the fact that a layer of insulation was added above the ceiling so that the temperature of the air in contact with the ceiling could vary with time. It may be seen that there are four discontinuous jumps in the horizontally averaged temperature fields in Fig. 9. The discontinuities occur at $z = 0.42$, 0.58, 0.98, and 1.24 m. At these locations, there are discontinuities in the shape of the mannequin: the lower surface of the mannequin's torso and upper legs (0.42 m), the top surface of the mannequin's upper legs (0.58 m), the mannequin's shoulders (0.9 m), and the top of the mannequin's head (1.24 m). At each of these positions, the air experiences a discontinuous increase in the amount of heated surface to which it is exposed.

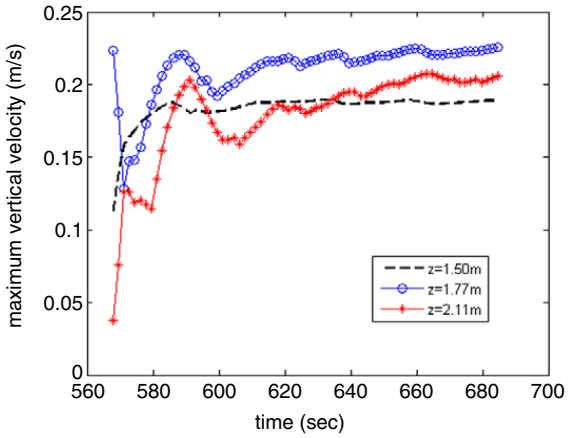

Fig. 5. The instantaneous vertical component of velocity, $v_z(t)$, is plotted as a function of time at three points above the mannequin's head.

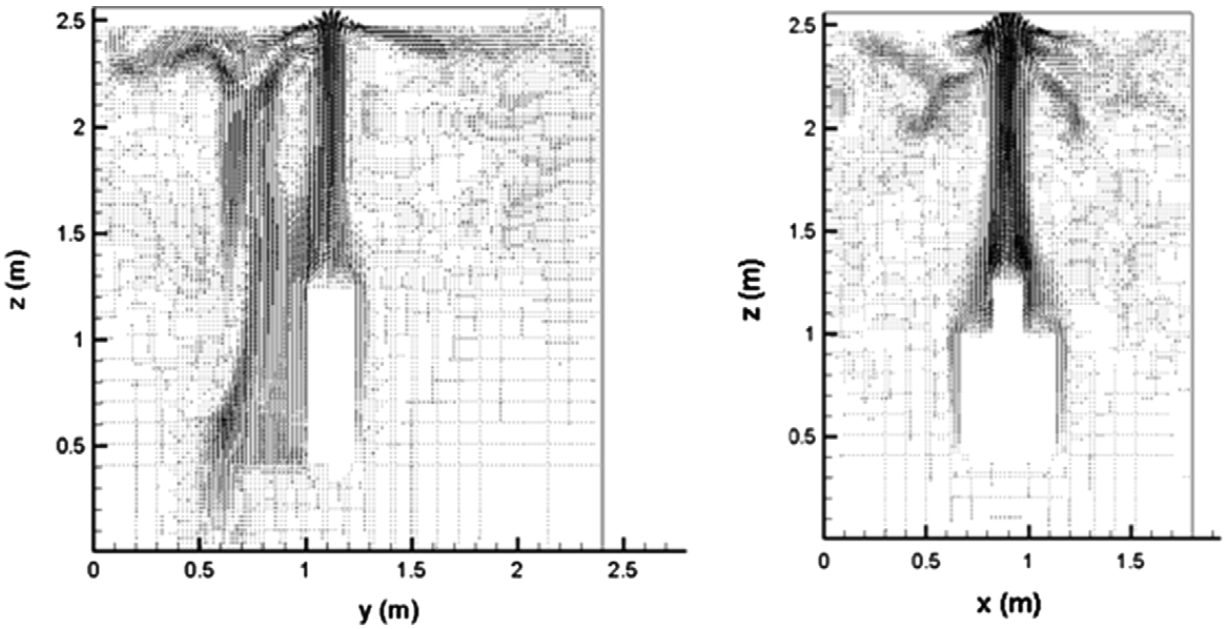

Fig. 6. The instantaneous velocity at $t = 143$ s is shown in the planes (a) $x = 0.9$ m and (b) $y = 1.12$ m.

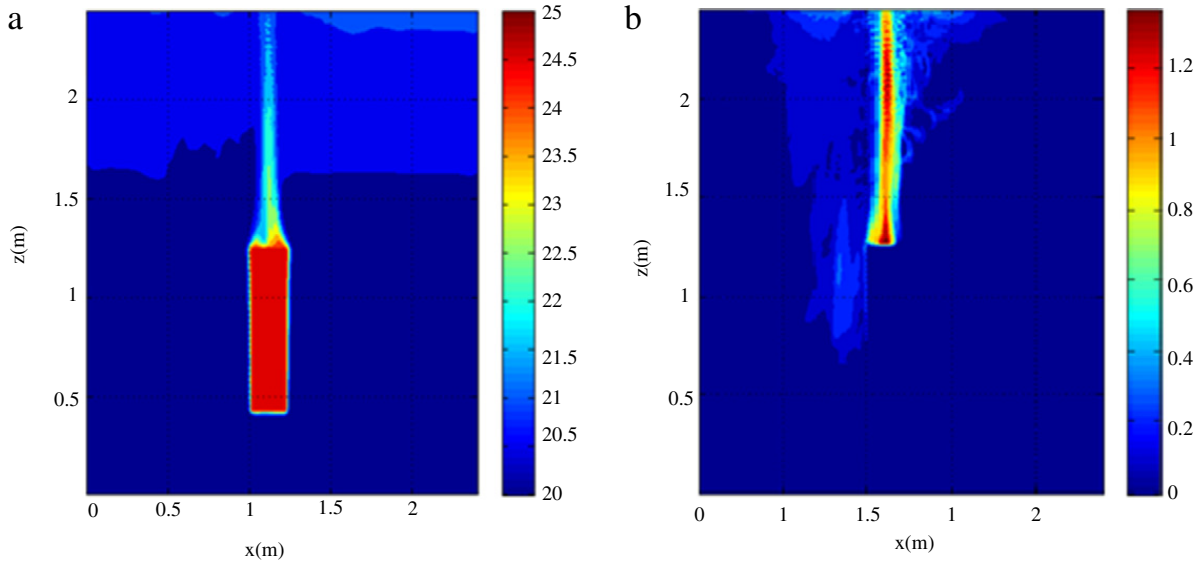

Fig. 7. The time-averaged temperature field (a) and the corresponding RMS fluctuations (b) are shown the geometrical symmetry plane of the room, $x = 0.9$ m.

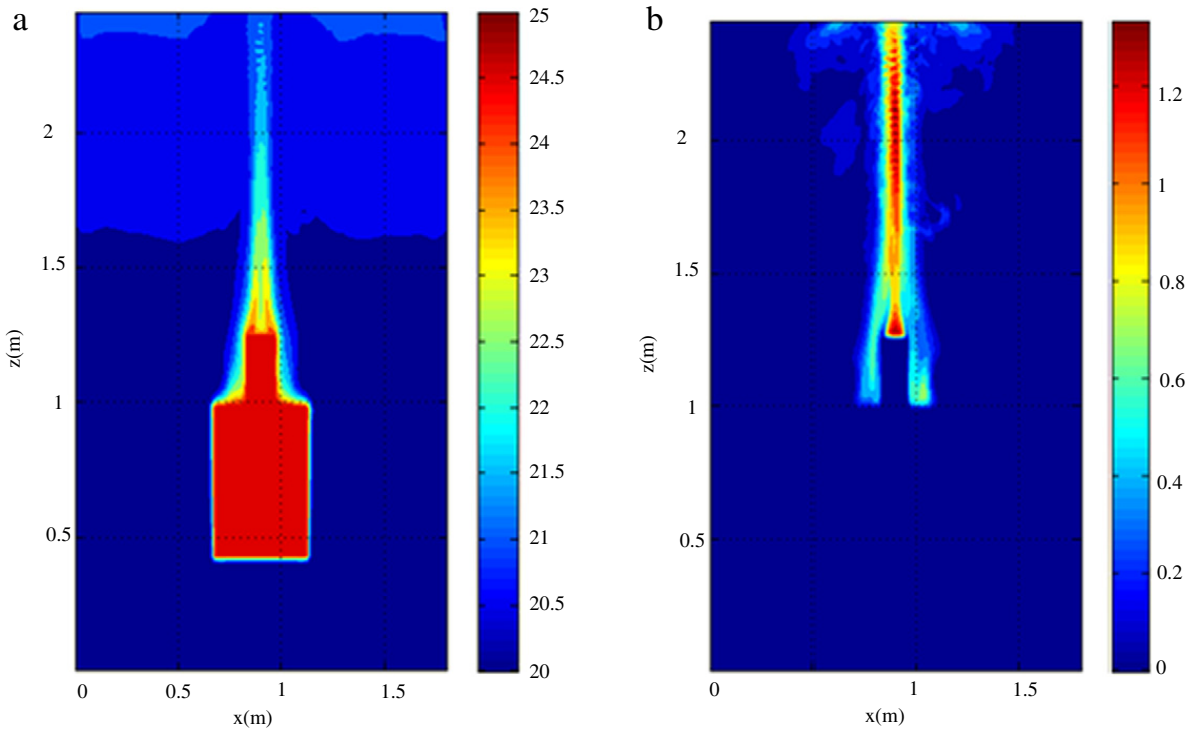

Fig. 8. The time-averaged temperature field (a) and the corresponding RMS fluctuations (b) are shown in the $y = 1.12$ m.

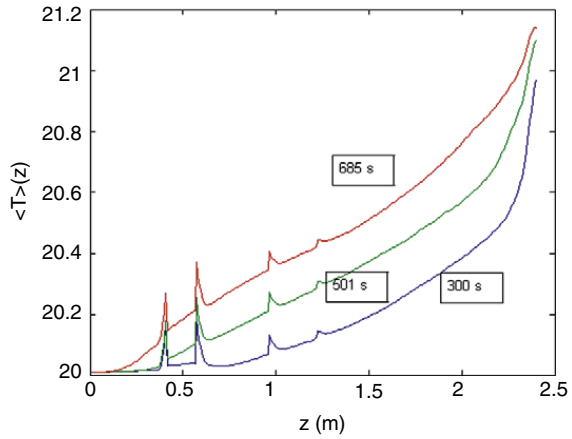

Fig. 9. The horizontally averaged air temperature is shown at three times.

Cravens and Settles defined the stratification parameter as follows:

$$S = \frac{\mathrm{d}T_\infty}{\mathrm{d}z\left(\frac{H}{T_S - T_{\infty,\frac{H}{2}}}\right)}. \tag{1}$$

In Eq. (1), H is the height of the person/mannequin, $\mathrm{d}T_\infty/\mathrm{d}z$ is the ambient temperature gradient, T_S is the average surface temperature of the person/mannequin, and $T_{\infty,H/2}$ is the air temperature at $H/2$. In their study, $S = 0.24$. As may be seen in Fig. 9, the air temperature is not linear even at 683 s, but if one roughly approximates the profile by a straight line, and takes $H = 1.24$ m, the value of S is roughly 0.12 for the simulation.

3.2. Particle tracking

The trajectories of 1000 small particles were computed after the velocity and temperature fields had reached a quasi-steady state. The particles were 5 μm in diameter and their density was 1000 kg/m^3. For particles of this size, Brownian motion is not important. The particle equation of motion included a nonlinear drag force and the gravitational force. The fluid velocity was interpolated from the grid points nearest to a particle to evaluate the fluid velocity at the location of

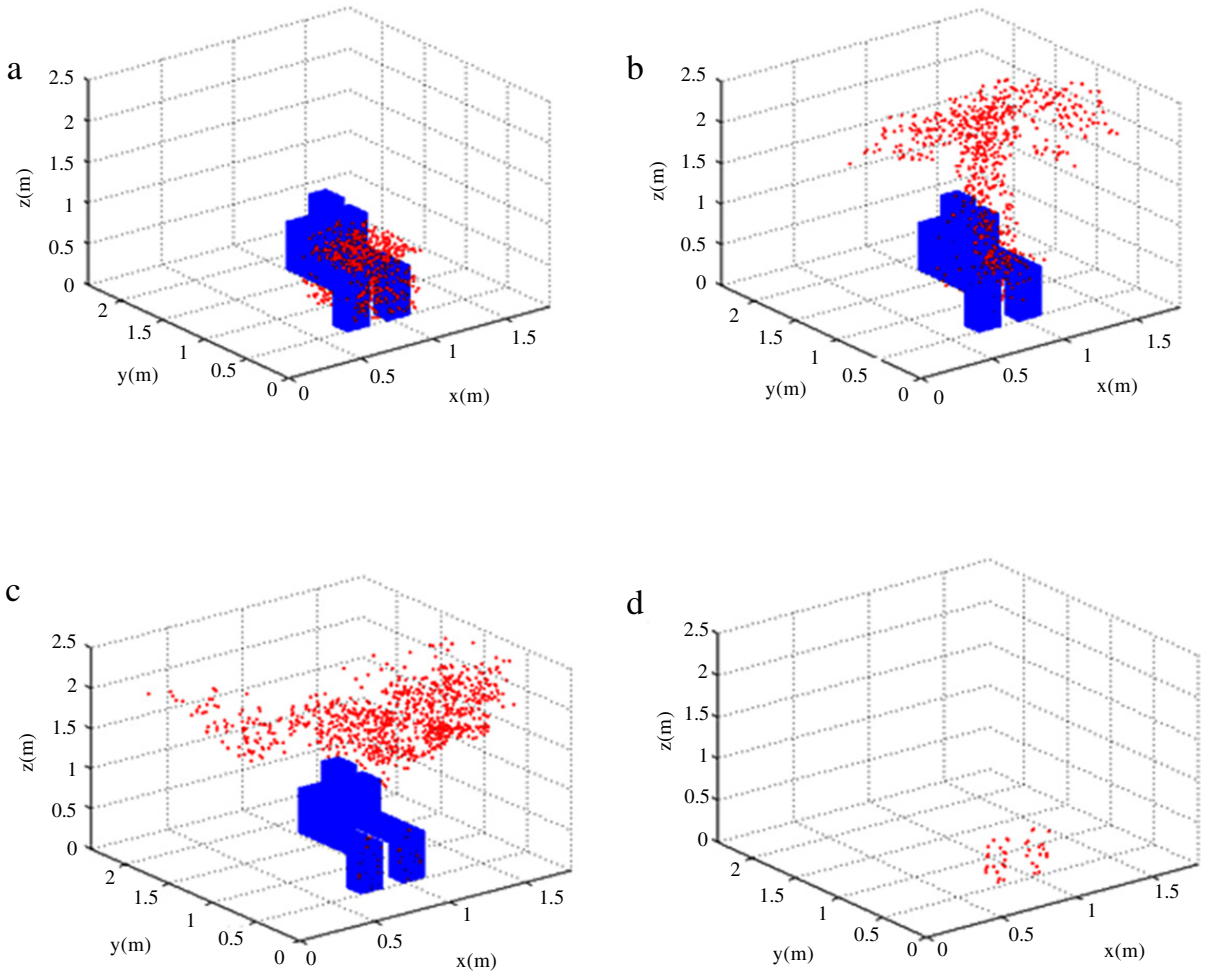

Fig. 10. The locations of the particles. (a) 1.67 s after they were released; (b) 25 s after they were released; (c) 166.7 s after they were released; (d) particles that deposited on the mannequin.

the particle. The feedback of the particles on the motion of the surrounding air was neglected because of the low particle concentration and the small size of the particles.

At $t = 133.4$ s, the particles were placed at random locations in a small rectangular volume directly in front of the mannequin's lower legs. The volume extended from 0.08 to 0.48 m above the floor, 0.68 to 1.12 m in the x direction, and 0.36 to 1.02 m in the y direction. For comparison, the width of the mannequin in the x direction is 0.44 m, and the height of the lower legs was 0.58 m. Therefore, the particles were distributed over a wider region in y and below the knees. The initial velocities of the particles were chosen to be the local fluid velocities. The particles were then tracked for 166.7 s. Panels (a) to (c) in Fig. 10 show the locations of the particles at 1.67, 25, and 166.7 s after the initial time of release. Several observations may be made by inspection of the figures. First, it may be seen that the flow is effective in carrying the particles upward and also drawing them toward the geometrical symmetry plane of the room ($y = 1.2$ m)—particles near the edges of the initial volume in the x direction are drawn inward and upward by the flow. This pumping action brings most of the particles, including particles that were initially close to the floor, upward to the mannequin's torso. In panel (b), it may be seen that the majority of the particles are close to the ceiling due to the action of the thermal plume. Some of the particles (38 out of 1000), however, deposit on the mannequin's lower legs and knees; the locations of these particles are shown in panel (d). Since breathing was not included in the simulation, it is not possible to determine how many of the particles would have been inhaled by the mannequin. Another striking feature of the particle distribution in panel (c) is the broad range over which particles are dispersed in the region near the ceiling.

4. Conclusions

Simulation results for the velocity and temperature fields inside a small room containing a heated mannequin have been presented in this paper. The results were obtained on a uniform spatial grid using a LBM. Results were obtained on three grids. The results obtained on the finest grid (grid space equal to 0.00667 m) agree well with results obtained by Craven and Settles in their experiments with a human subject. Specifically, the maximum values of the time-averaged vertical component of velocity for the simulation and the experiment were 0.226 m/s and 0.24 m/s, respectively. These values were

located at 0.53 m and 0.43 m above the mannequin's head, respectively. The stratification parameter was roughly the same as the experimental value for the period of time in which the time-averaging was performed for the simulation. Some of the discrepancies may be due to differences in geometry: a standing human subject in a large room versus an idealized model of a mannequin seated in a small room.

It is not clear that the results obtained on the highest resolution grid (grid 3) are grid independent. Further study will be needed to determine the requirements for grid independence. The values of the instantaneous global maximum for the vertical component of velocity show significant differences for grids 2 and 3. It is, however, true that, at larger times, the vertical velocities decrease substantially and this would presumably decrease the requirements for accurate simulations because the Reynolds number is smaller.

It is likely that the number of grid points could be reduced by a significant factor by using a coarser grid in the lower half of the room and in some portions of the upper half of the room. A fine grid would still be needed near the mannequin to resolve the thermal boundary layer. It would be more straightforward to implement such a variable grid using alternative numerical simulation techniques such as the finite volume method.

The results obtained by tracking 5 μm particles from a small volume near the floor and in front of the mannequin suggest that the mannequin's thermal plume is quite effective at bringing small particles close to the mannequin. A small fraction ($\sim$4%) of the particles deposited on the mannequin's lower legs during the simulation. Most of the remaining particles were distributed over a broad area near the ceiling at the end of the simulation. A longer simulation would be needed to determine how many of these particles deposit on the mannequin. It is expected that results for longer times as well as higher spatial and temporal resolution will be reported elsewhere.

Acknowledgments

The authors wish to acknowledge support for this work from the Syracuse Center of Excellence CARTI Program. The authors gratefully acknowledge the support and facilities of the NCSA at the University of Illinois.

References

[1] B. Cravens, G.S. Settles, A computational and experimental investigation of the human thermal plume, J. Fluids Eng. 128 (2006) 1251–1258.
[2] F.P. Incropera, D.P. DeWitt, Fundamentals of Heat and Mass Transfer, Wiley, New York, 2002.
[3] D. Marr, Velocity measurements in the breathing zone of a moving thermal manikin within the indoor environment, Ph.D. Thesis, Syracuse University, 2007.
[4] D.R. Marr, I.M. Spitzer, M.N. Glauser, Anisotropy in the breathing zone of a thermal manikin, Exp. Fluids 44 (2008) 661–673.
[5] I.M. Spitzer, D.R. Marr, M.N. Glauser, Impact of manikin motion on particle transport in the breathing zone, J. Aerosol Sci. 41 (2010) 373–383.
[6] A.M. Abdilghanie, L.R. Collins, D.A. Caughey, Comparison of turbulence modeling strategies for indoor flows, J. Fluids Eng. 131 (2009) 051402-1.
[7] L. Davidson, P.V. Nielsen, Large eddy simulation of the flow in three-dimensional ventilated room, in: Proceedings of the Fifth International Conference on Air Distribution in Rooms, Yokohama, Japan, 1996, pp. 161–168.
[8] W. Zhang, Q. Chen, Large eddy simulation of indoor airflow with a filtered dynamic subgrid scale model, Int. J. Heat Mass Transfer 43 (2000) 3219–3231.
[9] W. Zhang, Q. Chen, Large eddy simulation of natural and mixed convection airflow indoors with two simple filtered dynamic subgrid scale models, Numer. Heat Transfer A 37 (2000) 447–463.
[10] Y. Jiang, Q. Chen, Using large eddy simulation to study air-flows in and around buildings, ASHRAE Trans. 109 (2003) 517–526.
[11] T. Inamuro, T. Ogata, S. Tajima, N. Konishi, A lattice Boltzmann method for incompressible two-phase flows with large density differences, J. Comput. Phys. 198 (2004) 628–644.
[12] T. Inamuro, M. Yoshino, H. Inoue, R. Mizuno, F. Ogino, A lattice Boltzmann method for a binary miscible fluid mixture and its application to a heat-transfer problem, J. Comput. Phys. 179 (2002) 201–215.
[13] X. He, S. Chen, G.D. Doolen, A novel thermal model for the lattice Boltzmann method in incompressible limit, J. Comput. Phys. 146 (1998) 282.
[14] P. Lallemand, L.S. Luo, Hybrid finite-difference thermal lattice Boltzmann equation, Int. J. Mod. Phys. B 17 (2003) 41.
[15] P. Lallemand, L.S. Luo, Theory of the lattice Boltzmann method: acoustic and thermal properties in two and three dimensions, Phys. Rev. E 68 (2003) 036706.
[16] C.S. Nor Azwadi, T. Tanahashi, Development of 2-D and 3-D double population thermal lattice Boltzmann models, Matematika 24 (2008) 53–66.
[17] C.-H. Liu, K.-H. Lin, H.-C. Mai, C.-A. Lin, Thermal boundary conditions for thermal lattice Boltzmann simulations, Comput. Math. Appl. 59 (2010) 2178–2193.
[18] J. Derksen, H.E.A. Van den Akker, Large eddy simulations on the flow driven by a Rushton impeller, AIChE J. 45 (1999) 209–221.